Dinuclear Formamidinato Complexes of Nickel and Palladium

F. Albert Cotton,* Marek Matusz, Rinaldo Poli, and Xuejun Feng

Contribution from the Department of Chemistry and Laboratory for Molecular Structure and Bonding, Texas A&M University, College Station, Texas 77843. *Received June 15, 1987*

Abstract: The compounds $Ni_2(form)_4$ (**1**) and $Pd_2(form)_4$ (**2**), where form = $(p\text{-}CH_3C_6H_4)NCHN(p\text{-}CH_3C_6H_4)^-$, have been prepared and characterized by several physical methods, including X-ray crystallography. Both **1** and **2** form cubic crystals from CH_2Cl_2/hexane in the presence of moist air, with the composition $M_2(form)_4\cdot 2H_2O$. The space group is $Pn\bar{3}n$ and the unit cell edges are 20.841 (5) Å for **1** at 20 °C, 20.649 (2) Å for **1** at −105 °C, and 21.067 (4) Å for **2** at 25 °C. With 6 molecules in the unit cell, crystallographic symmetry 42 (D_4) is imposed. The principal dimensions of **1** (at 20 °C) and **2**, respectively, are as follows: torsion angles, 16.85°, 15.03°; M–M distances, 2.485 (2), 2.622 (3) Å; mean M–N distances, 1.904 (5), 2.063 (14) Å. The palladium compound was also crystallized as $Pd_2(form)_4\cdot(C_2H_5)_2O$ and its structure determined: space group $P4/ncc$ with a = 16.416 (2) Å, c = 23.827 (4) Å, and Z = 4. Refinement was not entirely successful because of disorder but the dimensions of the complex agreed well with those found in the H_2O-containing cubic crystals. Cyclic voltammetry showed that both compounds can be reversibly oxidized to the +1 state with $E_{1/2}$ values (vs Ag/AgCl) of +0.73 V for Ni and 0.81 V for Pd. For the palladium compound a second reversible oxidation was seen at +1.19 V but a second oxidation at ca. +1.25 V for the Ni compound was irreversible. Chemical oxidations to the $[M_2(form)_4]^+$ ions with $[Ag(CH_3CN)_2]BF_4$ and $AgPF_6$ allowed the isolation of the crystalline products $[Ni_2(form)_4]BF_4$ (**3**) and $[Pd(form)_4]PF_6$ (**4**), whose structures were determined; for **3**, space group $P4/n$ with a = 14.078 (3) Å, c = 13.379 (4) Å, and Z = 2; for **4**, space group $P4/ncc$ with a = 13.871 (5) Å, c = 29.180 (6) Å, and Z = 4. The $[Ni_2(form)_4]^+$ ion has an appreciably shorter Ni–Ni bond length, 2.418 (4) Å, than the neutral molecule and a much greater torsion angle, 27.4°. The $[Pd_2(form)_4]^+$ ion has a slightly longer Pd–Pd bond, 2.637 (6) Å, and slightly greater torsion angle, 17°, than the neutral molecule. SCF-Xα-SW calculations on the $M_2(HNCHNH)_4$ species indicate that there is little net M–M bonding. The EPR spectrum of the nickel cation indicates that the odd electron is in a metal-based MO, and the Xα calculation for $[Ni_2(HNCHNH)_4]^+$ suggests that this has partial δ^* character, thus explaining why electron loss from the neutral molecule results in bond shortening by ca. 0.07 Å. For $[Pd_2(form)_4]^+$ the EPR spectrum indicates that the odd electron occupies a ligand-based MO, and the Xα calculation is not inconsistent with this.

It is now known that compounds of the type I, containing M–M bonds of orders 1–4, can be formed by the metal atoms of groups VI (Cr, Mo, W), VII (Tc, Re), and VIII (Ru, Os, Rh, Ir, Pt).[1]

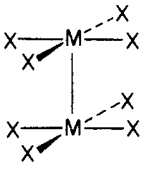

(I)

For Ir[II] the first such compound has only very recently been reported,[2] and we have also characterized a cobalt compound, $Co_2[(tol)N_3(tol)]_4$.[3] On the basis of the familiar orbital picture of metal–metal bond formation within this structural framework, we recognize a progression from a bond order of 4 when the metal atoms bring d^4 configurations to the compound down to a bond order of only 1 when two d^7 configurations come into play. These can be formally designated as $\sigma^2\pi^4\delta^2$ through $\sigma^2\pi^4\delta^2\delta^{*2}\pi^{*4}$ systems.

With the elements of the Ni, Pd, Pt group, several interesting questions led us to undertake the work reported in this paper. First, the only known M–M-bonded species, within the above definition of M–M bonding, were those of the d^7d^7 Pt_2^{6+} unit;[1b] no complexes of the M_2^{6+} unit and only one with the M_2^{5+} unit containing Ni or Pd have heretofore been described, and we wondered if additional M_2^{5+} species could not be isolated if the ligands were properly chosen.

Second, a few species of type I have been reported for Ni_2^{4+} and Pd_2^{4+} but the question of what sort of M–M bonding (if any) should be assumed to exist in them had not been conclusively answered. From the point of view alluded to above, these species should have $\sigma^2\pi^4\delta^2\delta^{*2}\pi^{*4}\sigma^{*2}$ configurations, and hence a bond order of zero. The compound $Pd_2(mhp)_4$ (mhp^- is the anion of 2-hydroxo-6-methylpyridine), with a Pd–Pd distance of 2.546 (1) Å, has been so described.[4] On the other hand, in the $M_2(dpt)_4$ molecules ($dpt^- = C_6H_5NNNC_6H_5^-$) the Ni–Ni and Pd–Pd distances (2.395 (3) and 2.563 (1) Å, respectively) have been regarded[5] as "very suggestive of metal–metal bonding", and the same authors also considered that "there seems little doubt on the basis of structural characteristics of the presence of metal–metal bonding in the ... nickel complexes $Ni_2(S_2CCH_2Ph)_4$ and $Ni_2(OSCPh)_4$, EtOH" whose structures had been previously reported[6,7] to contain relatively short Ni–Ni distances, namely, 2.50 and 2.56 Å, respectively. However, the expressed belief in the presence of these Ni^{II}–Ni^{II} or Pd^{II}–Pd^{II} bonds was not supported by any suggestion as to how (in orbital terms) they would be formed.

We shall describe here[8] experimental and theoretical investigations of a pair of nickel and palladium compounds, $M_2(form)_4$, and their cations, $[M_2(form)_4]^+$, from which we believe a good deal more understanding of such systems than has previously existed can be derived.

Experimental Section

Unless otherwise stated, all operations were carried out in standard Schlenkware under an inert atmosphere and by using carefully dried solvents. Instruments used were as follows: IR, Perkin-Elmer 783; ^1H NMR, Varian XL-200; EPR, Varian E-6S; CV and bulk electrolysis, BAS-100; UV/visible, Cary 17. Elemental analyses were by Galbraith Laboratories, Knoxville, TN. Hform,[9] $PhI\cdot Cl_2$,[10] and $[Ag(MeCN)_x]BF_4$[11] were prepared according to the literature. $Pd_3(OAc)_6$ and $AgPF_6$

(1) (a) Cotton, F. A.; Walton, R. A. *Multiple Bonds between Metal Atoms*; Wiley: New York, 1982. (b) Cotton, F. A.; Walton, R. A. *Struct. Bonding (Berlin)* **1985**, *62*, 1–49.
(2) Cotton, F. A.; Poli, R. *Polyhedron* **1987**, *6*, 1625.
(3) Cotton, F. A.; Poli, R. *Inorg. Chem.* **1987**, *26*, 3652.
(4) Clegg, W.; Garner, C. D.; Hassan Al-Samman, M. *Inorg. Chem.* **1982**, *21*, 1897.
(5) Corbett, M.; Hoskins, B. F.; McLeod, N. J.; O'Day, B. P. *Aust. J. Chem.* **1975**, *28*, 2377.
(6) Bonamico, M.; Dessy, G.; Fares, V. *Chem. Commun.* **1969**, *697*, 1106; *J. Chem. Soc., Dalton Trans.* **1977**, 2315.
(7) Melson, G. A.; Greene, P. T.; Bryan, R. F. *Inorg. Chem.* **1970**, *9*, 1116.
(8) A preliminary report of a portion of this work was given by: Cotton, F. A.; Matusz, M.; Poli, R. *Inorg. Chem.* **1987**, *26*, 1472.
(9) Roberts, R. M. *J. Organomet. Chem.* **1949**, *14*, 277.
(10) Lucas, H. J.; Kennedy, E. R. *Org. Synth.* **1955**, *3*, 482.

0002-7863/88/1510-1144$01.50/0

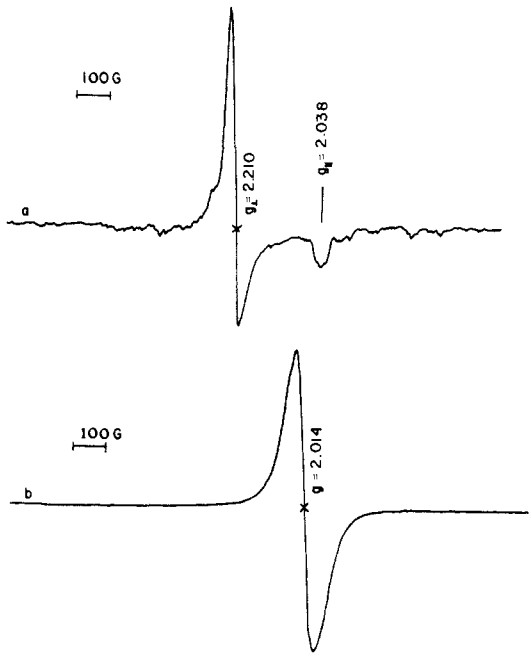

Figure 1. EPR spectra of $[M_2(form)_4]PF_6$ in CH_2Cl_2 glass at liquid nitrogen temperature: (a) M = Ni; (b) M = Pd.

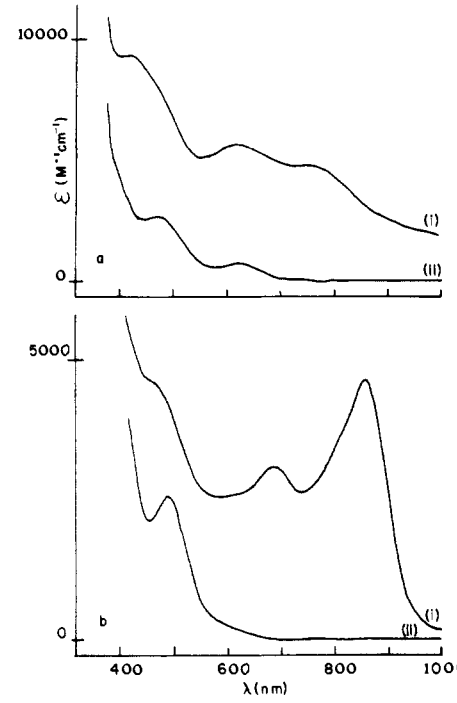

Figure 2. Visible spectra of $[M_2(form)_4]^{n+}$ in CH_2Cl_2: (a) M = Ni; (b) M = Pd. (i) n = 1; (ii) n = 0.

were purchased from Aesar and used as received.

Preparation of $Ni_2(form)_4 \cdot 2H_2O$. $NiBr_2$ (0.22 g, 1 mmol) was added to 20 mL of a THF solution of $Li^+(form)^-$ prepared in situ from Hform (0.9 g, 4 mmol) and 2.5 mL of 1.6 M solution of *n*-BuLi in hexane (4 mmol). The reaction mixture was stirred and refluxed for 24 h. It was cooled and filtered to give a microcrystalline, black product. Yield 0.25 g (ca. 40%). This material was dissolved in CH_2Cl_2, and *n*-hexane was added. Slow evaporation in air gave well-formed black cubes, which were shown by ^1H NMR and X-ray crystallography to be $Ni_2(form)_4 \cdot 2H_2O$. IR (Nujol mull/cm^{-1}): 1620 s, 1590 s, 1545 m, 1500 s, 1460 s, 1375 m, 1345 s, 1230 s, 1110 w, 970 m, 830 m, 820 m, 770 w, 535 m, 530 m, 475 w, 460 m. ^1H NMR ($CDCl_3$, δ): 1.67 (broad, H_2O, 4 H), 2.27 (s, C*H*$_3$, 24 H), 6.16 (s, NC*H*N, 4 H), 6.97–7.24 (m, aromatic, 32 H). The broad peak at 1.67 ppm disappeared when the sample was treated with D_2O. Integration suggested two water molecules per dimer. Anal. Calcd for $C_{60}H_{64}N_8Ni_2O_2$: Ni, 11.21; C, 68.85; H, 6.16. Found: Ni, 10.49; C, 70.27; H, 6.36. On one occasion a small quantity of needle-shaped crystals was obtained along with the cubes. Their spectral and electrochemical properties were identical with those of $Ni_2(form)_4 \cdot 2H_2O$. This material was not investigated further.

Oxidation of $Ni_2(form)_4$ to $Ni_2(form)_4^+$. (a) Electrochemical. $Ni_2(form)_4 \cdot 2H_2O$ (47.4 mg, 0.045 mmol) in 20 mL of a 0.2 M solution of *n*-Bu_4NPF_6 in CH_2Cl_2 was electrolyzed at 1.0 V vs Ag/AgCl as reference electrode. A 25-cm^2 Pt plate was used as a working electrode. After the consumption of 4.37 C (1 electron transferred, 100% yield) the electrolysis was stopped and the sample checked by cyclic voltammetry. A small amount of the neutral dimer was still present. Additional electrolysis showed small but steady current and was stopped after an additional 1 C of charge had passed through the solution. A control CV experiment showed the completeness of the oxidation process. The EPR spectrum of this solution is reported in Figure 1, while the UV/visible spectrum is shown in Figure 2.

(b) Chemical. $Ni_2(form)_4 \cdot 2H_2O$ (53 mg, 0.052 mmol) in 15 mL of CH_2Cl_2 was treated with a solution of $[Ag(CH_3CN)_2]BF_4$ (18.8 mg, 0.055 mmol). The reaction mixture immediately changed color from brown-yellow to dark green. It was stirred for 1 h at room temperature. The UV–vis spectrum indicated that the oxidation was complete. The solution was filtered through Celite to remove a fine precipitate of silver metal, and a layer of ether was placed over the filtrate. In a few days a crop a black cubes was collected by filtration. They were vacuum-dried. Yield ca. 30 mg. The IR spectrum showed a strong and very broad band at 1100 cm^{-1} (BF_4) and additional bands at 1500 w, 1460 s, 1380 s, 1320 s, 1260 m, 1220 m, 1010 w, 810 m, 790 m, 540 m, 480 m, 450 m, 430 m. The EPR spectrum of a frozen CH_2Cl_2 solution showed features identical with those of the sample obtained by electrochemical oxidation.

Preparation of $Pd_2(form)_4$. (a) $Pd_2(form)_4 \cdot 2THF$. $Pd_3(OAc)_6$ (0.96 g, 1.42 mmol) was added to a solution of $Li^+(form)^-$ in 100 mL of THF. The latter was prepared in situ by neutralizing Hform (2.014 g, 8.98 mmol) with a 1.6 M solution of *n*-BuLi in *n*-hexane (5.60 mL, 8.96 mmol). The mixture was stirred at room temperature for about 1 h. During that time the precipitation of a white solid followed by that of the orange microcrystalline product was observed. The mixture was warmed to the reflux temperature (the orange precipitate dissolved completely) and filtered hot. From the cooled solution 1.17 g of $Pd_2(form)_4 \cdot 2THF$ was recovered (43.7% yield). IR (Nujol mull/cm^{-1}): 1620 s, 1585 s, 1540 m, 1500 s, 1345 s, 1230 s, 1070 m, 965 m, 835 sh, 820 m, 545 w, 520 m, 450 m. Visible [CH_2Cl_2, λ_{max}/nm (ϵ/$mol^{-1} \cdot L \cdot cm$)]: 492 (2600). ^1H NMR ($CDCl_3$, δ): 1.84 (m, THF, 8 H), 2.24 (s, C*H*$_3$, 24 H), 3.74 (m, THF, 8 H), 6.87 (m, aromatic, 32 H), 7.05 (s, NC*H*N, 4 H). The mother liquor was evaporated to dryness to give an additional 1.09 g of impure material (total yield ca. 84%).

(b) $Pd_2(form)_4 \cdot C_6H_5CH_3$. $Pd_2(form)_4 \cdot 2THF$ (1.09 g) was recrystallized from 30 mL of hot toluene, affording 0.39 g of microcrystalline $Pd_2(form)_4 \cdot C_6H_5CH_3$, which separated out upon cooling to room temperature. The IR (Nujol mull) spectrum was identical with that of $Pd_2(form)_4 \cdot 2THF$, with the exception of the band at 1070 cm^{-1}, which was absent in the toluene adduct. ^1H NMR ($CDCl_3$, δ): 2.25 (s, C*H*$_3$, 24 H), 2.35 [s, C*H*$_3$ (toluene), 3 H], 6.88 (m, aromatic, 32 H), 7.05 (s, NC*H*N, 4 H), 7.19 [m, aromatic (toluene), 5 H].

(c) $Pd_2(form)_4 \cdot 2H_2O$. $Pd_2(form)_4 \cdot 2THF$ was dissolved in CH_2Cl_2, and *n*-hexane was carefully layered on top of it. This operation was conducted in air. Crystals of different shapes formed upon diffusion. The crystals were collected and dried in vacuo. Several of these became opaque, indicating probable loss of interstitial solvent. Others remained transparent. One of the latter was used for an X-ray analysis. A ^1H NMR analysis on a crop of handpicked crystals of this type ($CDCl_3$ solution) revealed the presence of water (broad peak at 1.59 ppm, which disappeared upon treatment with D_2O). Integration indicated 2 mol of H_2O per Pd dimer.

Oxidation of $Pd_2(form)_4$ to $[Pd_2(form)_4]^+$. (a) Electrochemical. $Pd_2(form)_4 \cdot 2THF$ (50 mg, 0.040 mmol) in 20 mL of CH_2Cl_2 was electrolyzed at 1.00 V vs Ag/AgCl. *n*-Bu_4NPF_6 (200 mg) was used as supporting electrolyte. A Pt plate (25 cm^2) was used as working electrode. The color changed from red-orange to very dark brown during the process. The current dropped after consumption of 4.8 C, and a control CV experiment confirmed the completeness of the oxidation process. The EPR spectrum of this solution is reported in Figure 1, while the UV/visible spectrum is in Figure 2.

(b) Chemical. (i) With $[Ag(MeCN)_2]BF_4$. $Pd_2(form)_4 \cdot C_6H_5CH_3$ (0.22 g, 0.17 mmol) in 20 mL of CH_2Cl_2 was treated with 62 mg of $Ag(MeCN)_2BF_4$ (0.22 mmol). The color immediately changed to very dark brown. After filtration through Celite, the solution was layered with

(11) Meerwein, H.; Hederich, V.; Wunderlich, K. *Arch. Pharm.* (*Weinheim, Ger.*) **1958**, *291*, 541. While the initial product contains 4 CH_3CN, two of these appear to be easily lost. We therefore write $(CH_3CN)_x$, $x \leq 4$, or $(CH_3CN)_2$, the latter being assumed in calculating molar quantities.

Table I. Crystal Data

	$Ni_2(form)_4 \cdot 2H_2O$					
formula	$C_{60}H_{64}N_8Ni_2O_2$	$C_{60}H_{64}N_8Ni_2O_2$	$C_{60}H_{64}N_8O_2Pd_2$	$C_{60}H_{60}BF_4N_8Ni_2$	$C_{64}H_{70}N_8Pd_2O$	$C_{60}H_{60}F_6N_8PPd_2$
fw	1046.65	1046.65	1142.04	1097.43	1180.12	1250.97
space group	$Pn\bar{3}n$	$Pn\bar{3}n$	$Pn\bar{3}n$	$P4/n$	$P4/ncc$	$P4/ncc$
systematic absences	$0kl$: $k + l \neq 2n$; hkk: $h \neq 2n$			$hk0$: $h + k \neq 2n$	$hk0$: $h + k \neq 2n$; $0kl$: $l \neq 2n$; hhl: $l \neq 2n$	
a, Å	20.841 (5)	20.649 (2)	21.067 (4)	14.078 (3)	16.416 (2)	13.871 (5)
c, Å				13.379 (4)	23.827 (4)	29.180 (6)
V, Å^3	9052 (4)	8848 (2)	9350 (5)	2652 (1)	6421 (3)	5617 (3)
Z	6	6	6	2	4	4
d_{calcd}, g/cm^3	1.152	1.178	1.217	1.374	1.221	1.479
crystal size, mm	0.45 × 0.45 × 0.6	0.3 × 0.3 × 0.4	0.1 × 0.2 × 0.35	0.1 × 0.2 × 0.05	0.4 × 0.4 × 0.4	0.1 × 0.1 × 0.1
μ(Mo Kα), cm^{-1}	6.692	9.129	6.109	7.723	5.938	7.233
data collection instrument	PĪ	CAD-4	CAD-4	Syntex P3	Syntex P3	CAD-4
radiation (monochromated in incident beam	Mo Kα (λ_α = 0.71073 Å)	Mo Kα (λ_α = 0.71073 Å)		Mo Kα (λ_α = 0.71073 Å)	Mo Kα (λ_α = 0.71073 Å)	
orientation reflections, no., range (2θ)	15	25	25, 10–30	25, 15–20	25, 20–35	25, 15–25
temp, °C	20	−105	25	22	20	20
scan method	ω	ω–2θ	ω	ω–2θ	ω	ω–$2\theta/\omega$
data collection range, 2θ, deg	4–45	4–45	4–50	4–47	4–50	4–45
no. of unique data, total with $F_o^2 > 3\sigma(F_o^2)^2$	1056, 521	1238, 548	656, 397	1040, 731	2143, 1653	1117, 559
no. of parameters refined	88	88	76	175		77
trans factors, max, min	1.0, 0.943	1.0, 0.9036	0.9964, 0.8824	1.0, 0.9036	0.9997, 0.9797	0.9974, 0.8995
R^a	0.04917	0.0672	0.0520	0.0480		0.0821
$R_w{}^b$	0.0620	0.0877	0.0649	0.0547		0.0984
quality-of-fit indicator[c]	1.236	1.967	1.41	0.907		1.94
largest shift/esd, final cycle	1.7[d]	0.014	0.56[d]	0.10		0.16
largest peak, e/Å	0.5	0.47	0.700	0.41		2.18

[a] $R = \sum||F_o| - |F_c||/\sum|F_o|$. [b] $R_w = [\sum w(|F_o| - |F_c|)^2/\sum w|F_o|^2)^{1/2}$; $w = 1/\sigma^2(|F_o|)$. [c] Quality of fit = $[\sum w(|F_o| - |F_c|)^2/(N_{obsd} - N_{parameters})]^{1/2}$. [d] This large shift was for a water molecule; largest shift for the dimer was <0.3.

Et_2O (10 mL). Diffusion caused the formation of orange crystals, while the color of the solution slowly turned orange. The crystals were collected (35 mg) and shown to be of an ether adduct of the dimer, $Pd_2(form)_4 \cdot OEt_2$, by their UV/visible and ^1H NMR properties.

(ii) With $AgPF_6$. $Pd_2(form)_4 \cdot 2THF$ (0.70 g, 0.56 mmol) was treated in 20 mL of CH_2Cl_2 with $AgPF_6$ (0.21 g, 0.83 mmol). The solution was filtered through Celite and layered with Et_2O (20 mL). Small black cubes of $[Pd_2(form)_4]PF_6$ formed upon diffusion. These were filtered off and dried under vacuum (0.18 g, 26%). The IR (Nujol mull) spectrum showed an intense and very broad band in the 4000–1700-cm^{-1} region. Additional bands were at 1580 s, 1560 s, 1490 m, 1410 m, 1320 s, 1295 m, 1275 s, 1220 s, 1160 s (broad), 1010 m, 940 m, 850 m, 830 m, 790 m, 710 w, 590 w, 570 w, 540 m, 520 m, and 415 w cm^{-1}. The compound is fairly air stable in the solid state, whereas its CH_2Cl_2 solutions were slightly air sensitive and gave back the neutral Pd(II) dimer upon long exposures. $[Pd_2(form)_4]PF_6$ was also reduced to $Pd_2(form)_4$ when reacted with dry n-Bu_4NBPh_4 in an attempt to carry out an ion metathesis reaction and when treated with anhydrous MeCN.

Attempted Oxidation of $Pd_2(form)_4$ with Cl_2. (a) In CH_2Cl_2. $Pd_2(form)_4 \cdot 2THF$ (0.12 g, 0.10 mmol) was dissolved in CH_2Cl_2 (10 mL) and treated with $PhI \cdot Cl_2$ (32 mg, 0.12 mmol). The color of the solution immediately changed from red-orange to dark red. Upon stirring at room temperature the color changed back to that of the original solution. The same behavior was observed upon subsequent treatment with an additional aliquot of $PhI \cdot Cl_2$. Visible spectroscopy confirmed that $Pd_2(form)_4$ was present in the final solution.

(b) In CCl_4. $Pd_2(form)_4 \cdot 2THF$ and $PhI \cdot Cl_2$ in equimolar amounts were mixed in CCl_4. No reaction took place at room temperature, at reflux, or upon irradiating the mixture with UV light, as shown by UV/visible monitoring.

X-ray Crystallography. (a) $Ni_2(form)_4 \cdot 2H_2O$. A single crystal was glued to the inside of a thin-walled glass capillary and mounted on the diffractometer. Crystal data are reported in Table I. The data collection was routine. An empirical absorption correction was applied according to the method described by North et al.[12] The structure was solved by the Patterson method and refined by alternate cycles of full-matrix least-squares and difference Fourier maps with the Enraf-Nonius SDP package. All the non-hydrogen atoms were refined anisotropically, and hydrogen atoms were added at calculated positions and included in the structure factor calculations. Their isotropic thermal parameter was refined, while their positional coordinates were constrained to ride on those of the corresponding carbon atoms. At this point a strong peak was still present in the difference Fourier map on the fourfold axis. Chemical evidence obtained from the NMR experiments had shown that this compound contains water. The peak was therefore assigned to a full occupancy oxygen atom, corresponding to the H_2O/dimer ratio indicated by the NMR spectrum. This refined with a very high thermal parameter but it improved substantially the R value and the quality-of-fit indicator (see Table I for details). This oxygen atom is not connected to the dinuclear molecule (Ni–O distance = 5.548 Å) and it is close to a crystallographic 432 center so that six oxygen atoms are close to each other in an octahedral arrangement, but at a distance (5.134 Å) too long for a hydrogen-bonding interaction. Competing tendencies to form hydrogen bonds and to occupy fully the free volume left after packing of the nickel dimers may be responsible for the large thermal displacements of this part of the structure (see Results for further details). In an effort to resolve this problem we redetermined the structure from data collected

Table II. Positional Parameters and Their Estimated Standard Deviations for $Ni_2(form)_2 \cdot 2H_2O$ at 20 °C

atom	x	y	z	B, Å^2
Ni	0.7500	0.30963 (7)	0.7500	3.63 (3)
O	0.7500	0.576 (3)	0.7500	52 (3)[a]
N	0.6956 (3)	0.3045 (3)	0.6768 (3)	3.9 (1)
C1	0.6655 (3)	0.2500	0.6655 (3)	4.4 (2)
C10	0.6877 (3)	0.3532 (3)	0.6304 (4)	4.1 (2)
C11	0.6784 (4)	0.4164 (4)	0.6499 (4)	5.2 (2)
C12	0.6683 (4)	0.4630 (4)	0.6045 (5)	6.1 (2)
C13	0.6689 (4)	0.4504 (5)	0.5394 (5)	6.4 (3)
C14	0.6809 (5)	0.3887 (5)	0.5204 (4)	6.8 (3)
C15	0.6913 (4)	0.3399 (4)	0.5647 (4)	5.4 (2)
C16	0.6566 (5)	0.5023 (6)	0.4893 (6)	9.7 (3)
H1	0.629 (4)	0.2500	0.629 (4)	8 (1)[a]
H11	0.6778 (4)	0.4281 (4)	0.7004 (4)	8 (1)[a]
H12	0.6609 (4)	0.5122 (4)	0.6192 (5)	8 (1)[a]
H14	0.6836 (5)	0.3767 (5)	0.4701 (4)	8 (1)[a]
H15	0.6991 (4)	0.2913 (4)	0.5486 (4)	8 (1)[a]
H161	0.6487 (5)	0.5476 (6)	0.5134 (6)	15 (3)[a]
H162	0.6127 (5)	0.4894 (6)	0.4650 (6)	15 (3)[a]
H163	0.6948 (5)	0.5073 (6)	0.4547 (6)	15 (3)[a]

[a] These atoms were refined isotropically. Anisotropically refined atoms are given in the form of the equivalent isotropic displacement parameter defined as $(4/3)[a^2\beta_{11} + b^2\beta_{22} + c^2\beta_{33} + ab(\cos\gamma)\beta_{12} + ac(\cos\beta)\beta_{13} + bc(\cos\alpha)\beta_{23}]$.

(12) North, A. C. T.; Phillips, D. C.; Mathews, F. S. *Acta Crystallogr., Sect. A* **1968**, *A24*, 351.

Table III. Positional Parameters and Their Estimated Standard Deviations for $Ni_2(form)_4 \cdot 2H_2O$ at −105 °C

atom	x	y	z	B, Å²
Ni	0.7500	0.3102 (1)	0.7500	3.97 (5)
O	0.7500	0.577 (2)	0.7500	31 (2)[a]
N	0.6954 (4)	0.3048 (4)	0.6765 (4)	4.2 (2)
C1	0.6645 (5)	0.2500	0.6645 (5)	4.5 (2)
C10	0.6874 (5)	0.3545 (5)	0.6292 (5)	4.0 (3)
C11	0.6794 (5)	0.4177 (4)	0.6485 (5)	4.4 (3)
C12	0.6708 (5)	0.4654 (5)	0.6044 (6)	5.0 (3)
C13	0.6697 (6)	0.4527 (6)	0.5379 (7)	6.1 (4)
C14	0.6793 (6)	0.3897 (6)	0.5185 (6)	6.1 (4)
C15	0.6894 (6)	0.3404 (5)	0.5624 (6)	5.2 (3)
C16	0.6567 (7)	0.5056 (7)	0.4877 (6)	8.1 (4)
H1	0.617 (5)	0.2500	0.617 (5)	7 (1)[a]
H11	0.6788 (5)	0.4293 (4)	0.6990 (5)	7 (1)[a]
H12	0.6634 (5)	0.5145 (5)	0.6191 (6)	7 (1)[a]
H14	0.6820 (6)	0.3777 (6)	0.4681 (6)	7 (1)[a]
H15	0.6972 (6)	0.2918 (5)	0.5463 (6)	7 (1)[a]
H161	0.6631 (7)	0.5566 (7)	0.4957 (6)	21 (4)[a]
H162	0.6110 (7)	0.4989 (7)	0.4642 (6)	21 (4)[a]
H163	0.6946 (7)	0.4878 (7)	0.4573 (6)	21 (4)[a]

[a] These atoms were refined isotropically. Anisotropically refined atoms are given in the form of the equivalent isotropic displacement parameter defined as $(4/3)[a^2\beta_{11} + b^2\beta_{22} + c^2\beta_{33} + ab(\cos\lambda)\beta_{12} + ac(\cos\beta)\beta_{13} + bc(\cos\alpha)\beta_{23}]$.

at a lower (−105 ± 1 °C) temperature. As expected the cell was slightly smaller than that measured at room temperature, indicating tighter packing. The isotropic displacement parameter, *B*, of the oxygen atom dropped from 52 to 31 Å². Relevant distances concerning the oxygen atom were as follows: Ni···O, 5.522 Å; O···O, 5.054 Å. Fractional atomic coordinates are listed in Table II for the room-temperature structure and in Table III for the low-temperature one. Selected bond distances and angles are reported in Table IV.

(b) $Pd_2(form)_4 \cdot 2H_2O$. A single crystal was glued to the tip of a glass fiber and mounted on the diffractometer. Crystal data are assembled in Table I. The crystal is isostructural with that of $Ni_2(form)_4 \cdot 2H_2O$ (vide supra). Data were reduced as previously described for $Ni_2(form)_4 \cdot 2H_2O$. The structure was solved and refined as described for the corresponding nickel complex, except for the phenyl ring, which was refined as a perfect hexagon (C–C = 1.395 Å), and the same behavior was observed; i.e., a strong peak remained in the difference Fourier map at the end of the refinement on $Pd_2(form)_4$. The peak is close to the crystallographic 432 special position, thus generating a total of six such peaks in an octahedral arrangement. A contour map of electron density calculated in a plane containing four of these peaks is shown in Figure 3. The peak was identified as an oxygen atom on the basis of chemical evidence and by analogy with the nickel complex. This refined with a very high isotropic thermal parameter (B = 43 Å²) but it was otherwise well-behaved. Distances were as follows: Pd···O, 5.646 Å; O···O, 5.056 Å. Fractional atomic coordinates are in Table V, while selected bond distances and angles are in Table IV.

(c) $Pd_2(form)_4 \cdot OEt_2$. A single crystal was glued to the tip of a glass fiber and mounted on the diffractometer. Crystal data are in Table I. The data collection and reduction and the structure solution and refinement were carried out as previously described for $M_2(form)_4 \cdot 2H_2O$ (M = Ni, Pd). The refinement was smooth on the molecule of the dimer, allowing the agreement factor to reach 0.13 for the anisotropic model. At this point several peaks showed up in the difference Fourier map around the $\bar{4}$ position. The ^1H NMR spectrum indicated that one molecule of Et_2O per dimer was present, and packing considerations were consistent with it occupying that region of space in the unit cell. The symmetry of the special position is, however, higher than that of the molecule so that disorder was expected. No reasonable disordered model could be successfully refined. We concluded that the ether molecule is presumably distributed among several positions, and we did not attempt to model this electron density any further on the grounds that we already had a successfully refined structure for the water adduct of the same dimer. At the 0.13 level for the agreement factor, the palladium–palladium distance was 2.635 (3) Å. The other distances and angles in the dimer agree well with those found for the crystal containing water. The fractional atomic coordinates for the palladium dimer in this structure are included in the Supplementary Material.

(d) $[Ni_2(form)_4]BF_4$. A small regular crystal was glued to the tip of a glass fiber and mounted on the diffractometer. Crystal data are reported in Table I. The axial dimensions and the Laue class ($4/m$) were confirmed by axial photographs. Systematic absences from the data uniquely determined the space group as $P4/n$. The structure was solved

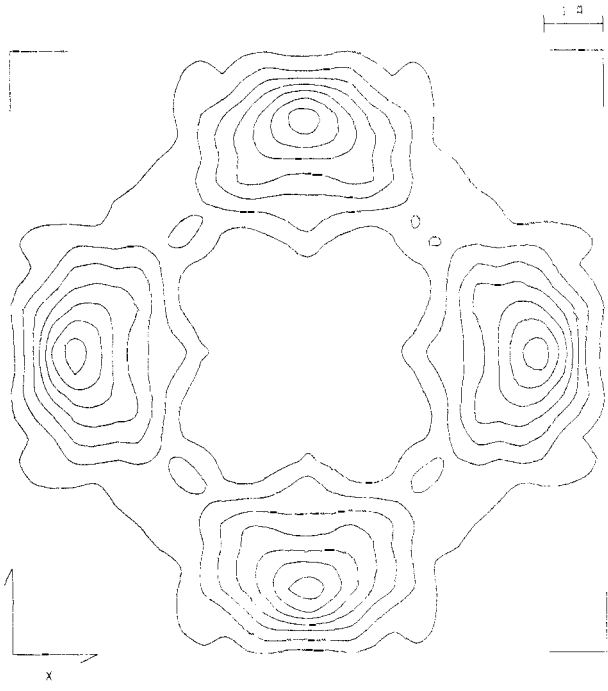

Figure 3. Contour map of the residual electron density around the crystallographic 432 center at the end of refinement on $Pd_2(form)_4$. A section across the xy plane with z = 0.75 is shown.

by the Patterson interpretation program provided by SHELX-86.[13] All of the non-hydrogen atoms of the dinuclear cation were refined anisotropically. Hydrogen atoms were included at calculated distances and used for the structure factor calculations but not refined. To avoid instability, the phenyl rings were constrained to be perfect hexagons (C–C = 1.395 Å). Calculations were performed with the SHELX-76 package.[14] At the end of the refinement of the $[Ni_2(form)_4]^+$ ion, the top peak of a difference Fourier map appeared on a fourfold axis, halfway between the nickel atoms of two different units. Two additional peaks were found on the same axis on both sides of the top peak, at a distance corresponding to B–F bonds. These peaks were introduced in the model as one boron and two half-occupancy fluorine atoms and refined. A subsequent difference Fourier map showed additional peaks. A total of 26 partial fluorine atoms is present because of the disorder, 8 of which are independent. The disorder is schematically illustrated

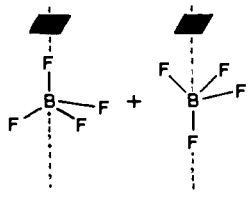

The fluorine atoms were assigned appropriate occupancy factors according to the symmetry and the number of fluorine atoms in the molecule and refined. The model, although it appears awkward, refined surprisingly well, giving final R = 0.048 and R_w = 0.055. Fractional atomic coordinates are listed in Table VI, while selected bond distances and angles are reported in Table IV.

(e) $[Pd_2(form)_4]PF_6$. Several crystals of this compound were investigated during the preliminary cell constant determination and none was found to be single. They systematically showed clusters of spots in the rotation photographs, indicating serious twinning problems. A single crystal, eventually obtained by cutting a bigger crystal and selecting one of the smallest fragments, was glued to the tip of a glass fiber and mounted on the diffractometer. Crystal data are reported in Table I. No decay of intensity in three standard reflections was observed during data collection. The solution and refinement of the structure did not proceed routinely for the following reason. Data were first collected by employing a cell with only half of the true c dimension. This happened because the layers with l odd are systematically weak (this being due to all of the heavy atoms being on the crystallographic fourfold axes; see *International*

(13) Sheldrick, G. M. "SHELXS-86", Institut für Anorganische Chemie der Universität, Göttingen, F.R.G., 1986.
(14) Sheldrick, G. M. "SHELX-76", University of Cambridge, 1976.

Table IV. Selected Bond Distances (Å) and Angles (Deg) for $M_2(form)_4 \cdot 2H_2O$ (M = Ni, Pd) and $[M_2(form)_4]X$ (M = Ni, X = BF_4; M = Pd, X = PF_6)

	$Ni_2(form)_4 \cdot 2H_2O$				
	room temp	low temp	$[Ni_2(form)_4]BF_4$	$Pd_2(form)_4 \cdot 2H_2O$	$[Pd_2(form)_4]PF_6$
M-M	2.485 (2)	2.491 (3)	2.418 (4)	2.622 (3)	2.637 (6)
M-N	1.904 (5)	1.898 (8)	1.924 (8)	2.063 (14)	2.03 (2)
			1.920 (8)		2.05 (3)
M···F			4.297 (3)		4.36 (5)
			4.401 (3)		4.46 (4)
M-M-N	86.8 (2)	86.6 (2)	86.0 (3)	85.0 (3)	86.7 (7)
			86.2 (3)		84.4 (6)
trans-N-M-N	173.6 (2)	173.2 (3)	170.0 (4)	170.0 (4)	173 (1)
			172.0 (4)		168.9 (8)
cis-N-M-N	89.8 (2)	89.8 (3)	86.0 (3)	89.6 (5)	89.8 (9)
			89.7 (3)		89 (1)
N-M-M-N[a]	16.8 (3)	16.8 (3)	27.4 (4)	15.1 (6)	17 (1)

[a] Torsion angle.

Table V. Positional Parameters and Their Estimated Standard Deviations for $Pd_2(form)_4 \cdot 2H_2O$

atom	*x*	*y*	*z*	*B*, Å^2
Pd	0.7500	0.31223 (9)	0.7500	4.39 (5)
N	0.6907 (6)	0.3037 (5)	0.6726 (7)	4.4 (4)
C1	0.6627 (6)	0.2500	0.6627 (6)	4.7 (4)
C10	0.6847 (5)	0.3532 (5)	0.6277 (5)	4.4 (4)
C11	0.6751 (5)	0.4154 (5)	0.6482 (5)	5.0 (4)
C12	0.6660 (5)	0.4638 (5)	0.6038 (5)	5.8 (5)
C13	0.6665 (5)	0.4499 (5)	0.5391 (5)	6.8 (7)
C14	0.6761 (5)	0.3876 (5)	0.5187 (5)	7.4 (6)
C15	0.6852 (5)	0.3393 (5)	0.5630 (5)	5.8 (5)
C16	0.656 (1)	0.5027 (9)	0.484 (1)	9.6 (7)
O	0.7500	0.580 (4)	0.7500	43 (3)[a]
H1	0.6245	0.2500	0.6245	10 (3)[a]
H11	0.6747 (5)	0.4262 (5)	0.6983 (5)	10 (3)[a]
H12	0.6586 (5)	0.5120 (5)	0.6196 (5)	10 (3)[a]
H14	0.6764 (5)	0.3768 (5)	0.4685 (5)	10 (3)[a]
H15	0.6926 (5)	0.2910 (5)	0.5472 (5)	10 (3)[a]
H161	0.639 (1)	0.5027 (9)	0.533 (1)	9 (3)[a]
H162	0.615 (1)	0.5021 (9)	0.453 (1)	9 (3)[a]
H163	0.684 (1)	0.5448 (9)	0.476 (1)	9 (3)[a]

[a] These atoms were refined isotropically. Anisotropically refined atoms are given in the form of the equivalent isotropic displacement parameter defined as $(4/3)[a^2\beta_{11} + b^2\beta_{22} + c^2\beta_{33} + ab(\cos\gamma)\beta_{12} + ac(\cos\beta)\beta_{13} + bc(\cos\alpha)\beta_{23}]$.

Tables for X-ray Crystallography[15]) and were therefore missed during the indexing procedure and axial photographs. The problem had been worsened by the small dimensions of the crystal. Volume considerations and comparison with the results found for tetragonal $Pd_2(form)_4 \cdot OEt_2$ (which also showed systematically weak layers for *l* odd) raised the possibility that the *c* axis had to be doubled, and this was confirmed after examining an axial photograph with a longer exposure time. The layers with *l* odd were then collected, and the two data sets were merged with SHELX; an agreement factor of 9% was obtained. The structure was solved by the Patterson interpretation program of the SHELXS-86 package[13] and refined with cycles of full-matrix least squares. The limited number of observations allowed anisotropic refinement of only the palladium, phosphorus, and fluorine atoms, and the phenyl rings were constrained to be perfect hexagons (C-C = 1.395 Å) in order to keep the number of parameters low. The hydrogen atoms were introduced at the calculated positions and constrained to ride on the corresponding carbon atoms during the refinement. The final agreement factor *R* was 0.082 (R_w = 0.098). Ghost peaks appeared in the last difference Fourier map on the fourfold axis about midway between each palladium atom and the fluorine atom of the PF_6^- ion. They were at chemically unreasonable positions and were considered to be the result of series termination errors due to the bad resolution along the *c* axis. Fractional atomic coordinates are reported in Table VII, while selected bond distances and angles are listed in Table IV.

Computational Procedures. The calculations were carried out by the SCF-Xα-SW method[16,17] employing a program written by M. Cook of Harvard University with modifications made locally by B. E. Bursten and G. G. Stanley. The real $M_2(form)_4$ molecules were modeled by $M_2(HNCHNH)_4$ molecules. The actual $M_2(form)_4$ molecules have torsion angles of 16.85° (Ni) and 15.03° (Pd) about the M-M bonds and thus have D_4 symmetry, and calculations were done in this symmetry. However, to take advantage of certain properties of the higher symmetry, D_{4h}, and to facilitate comparison of results with those previously obtained for other compounds, calculations were also done for the $M_2(HNCHNH)_4$

Table VI. Positional Parameters and Their Estimated Standard Deviations for $[Ni_2(form)_4]^+BF_4^-$

atom	*x*	*y*	*z*	*B*, Å^2
Ni1	0.2500	0.2500	0.6539 (2)	3.04 (7)
Ni2	0.2500	0.2500	0.4732 (2)	2.68 (7)
N1	0.1667 (6)	0.1425 (6)	0.6438 (7)	3.0 (2)
N2	0.2254 (6)	0.1159 (6)	0.4826 (7)	3.2 (2)
C1	0.1763 (6)	0.0899 (7)	0.563 (1)	3.3 (3)
C10	0.0925 (4)	0.1237 (5)	0.7123 (6)	3.2 (3)
C11	0.1062 (4)	0.1440 (5)	0.8134 (6)	4.2 (3)
C12	0.0340 (4)	0.1254 (5)	0.8821 (6)	4.4 (3)
C13	−0.0518 (4)	0.0865 (5)	0.8498 (6)	4.4 (3)
C14	−0.0654 (4)	0.0662 (5)	0.7487 (6)	4.2 (3)
C15	0.0067 (4)	0.0848 (5)	0.6800 (6)	3.5 (3)
C16	−0.1304 (9)	0.067 (1)	0.926 (1)	6.7 (4)
C20	0.2637 (5)	0.0468 (4)	0.4174 (5)	2.6 (3)
C21	0.2880 (5)	0.0716 (4)	0.3198 (5)	3.6 (3)
C22	0.3241 (5)	0.0030 (4)	0.2548 (5)	3.8 (3)
C23	0.3359 (5)	−0.0904 (4)	0.2876 (5)	4.6 (4)
C24	0.3116 (5)	−0.1151 (4)	0.3852 (5)	4.7 (3)
C25	0.2755 (5)	−0.0465 (4)	0.4502 (5)	3.8 (3)
C26	0.375 (1)	−0.1649 (9)	0.215 (1)	6.0 (4)
B	0.7500	0.7500	−0.0590	8[a]
F1	0.7500	0.7500	0.0249	5[a]
F2	0.7500	0.7500	−0.1442	20[a]
Fa	0.6576	0.6989	−0.0931	3[a]
Fb	0.6524	0.7787	−0.0995	5[a]
Fc	0.6412	0.7458	−0.0365	6[a]
Fd	0.6784	0.6535	−0.0733	3[a]
Fe	0.7048	0.6993	0.0017	4[a]
Ff	0.6950	0.7404	−0.1441	3[a]
H1	0.1423 (6)	0.0211 (7)	0.562 (1)	5.6 (9)[a]
H11	0.1726 (4)	0.1741 (5)	0.8384 (6)	5.6 (9)[a]
H12	0.0445 (4)	0.1412 (5)	0.9603 (6)	5.6 (9)[a]
H14	−0.1318 (4)	0.0361 (5)	0.7236 (6)	5.6 (9)[a]
H15	−0.0037 (4)	0.0691 (5)	0.6017 (6)	5.6 (9)[a]
H161	−0.0985 (9)	0.069 (1)	1.000 (1)	9 (1)[a]
H162	−0.1592 (9)	−0.003 (1)	0.913 (1)	9 (1)[a]
H163	−0.1868 (9)	0.119 (1)	0.922 (1)	9 (1)[a]
H21	0.2789 (5)	0.1438 (4)	0.2944 (5)	5.6 (9)[a]
H22	0.3429 (5)	0.0221 (4)	0.1792 (5)	5.6 (9)[a]
H24	0.3206 (5)	−0.1874 (4)	0.4106 (5)	5.6 (9)[a]
H25	0.2566 (5)	−0.0656 (4)	0.5258 (5)	5.6 (9)[a]
H261	0.441 (1)	−0.1391 (9)	0.183 (1)	9 (1)[a]
H262	0.328 (1)	−0.1865 (9)	0.155 (1)	9 (1)[a]
H263	0.390 (1)	−0.2250 (9)	0.262 (1)	9 (1)[a]

[a] These atoms were refined isotropically. Anisotropically refined atoms are given in the form of the isotropic equivalent displacement parameter defined as $(4/3)[a^2\beta_{11} + b^2\beta_{22} + c^2\beta_{33} + ab(\cos\gamma)\beta_{12} + ac(\cos\beta)\beta_{13} + bc(\cos\alpha)\beta_{23}]$.

(15) Hahn, T., Ed. *International Tables for Crystallography*; D. Reidel: Dordrecht, 1983; Vol. A; p 440–443.
(16) Johnson, K. H. *Adv. Quantum Chem.* **1973**, *7*, 143.
(17) Slater, J. C. *Quantum Theory of Molecules and Solids*; McGraw-Hill: New York, 1974; Vol. IV.

Table VII. Positional Parameters and Their Estimated Standard Deviations for $[Pd_2(form)_4]^+PF_6^-$

atom	*x*	*y*	*z*	*B* Å^2
Pd1	0.2500	0.2500	0.2237 (2)	2.3 (1)
Pd2	0.2500	0.2500	0.3140 (2)	2.3 (1)
N1	0.178 (2)	0.377 (2)	0.2277 (9)	3.5 (5)[a]
N2	0.143 (2)	0.351 (2)	0.3072 (7)	2.5 (4)[a]
C1	0.135 (2)	0.398 (2)	0.2703 (9)	2.8 (6)[a]
C10	0.078 (1)	0.370 (1)	0.3435 (6)	2.8 (7)[a]
C11	0.112 (1)	0.367 (1)	0.3886 (6)	3.3 (7)[a]
C12	0.049 (1)	0.389 (1)	0.4246 (6)	3.0 (7)[a]
C13	−0.047 (1)	0.412 (1)	0.4155 (6)	3.6 (7)[a]
C14	−0.080 (1)	0.414 (1)	0.3704 (6)	3.7 (7)[a]
C15	−0.017 (1)	0.393 (1)	0.3344 (6)	3.1 (7)[a]
C16	−0.119 (3)	0.433 (3)	0.455 (1)	6 (1)[a]
C20	0.176 (1)	0.448 (1)	0.1938 (6)	3.3 (7)[a]
C21	0.167 (1)	0.418 (1)	0.1484 (6)	2.1 (6)[a]
C22	0.154 (1)	0.486 (1)	0.1136 (6)	3.0 (7)[a]
C23	0.151 (1)	0.584 (1)	0.1243 (6)	3.6 (7)[a]
C24	0.160 (1)	0.614 (1)	0.1697 (6)	3.8 (8)[a]
C25	0.172 (1)	0.546 (1)	0.2045 (6)	4.7 (8)[a]
C26	0.131 (3)	0.660 (2)	0.089 (1)	6 (1)[a]
H1	0.089 (2)	0.461 (2)	0.2719 (9)	8 (3)[a]
H11	0.186 (1)	0.349 (1)	0.3958 (6)	8 (3)[a]
H12	0.074 (1)	0.386 (1)	0.4595 (6)	8 (3)[a]
H14	−0.154 (1)	0.433 (1)	0.3629 (6)	8 (3)[a]
H15	−0.042 (1)	0.396 (1)	0.2992 (6)	8 (3)[a]
H161	−0.065 (3)	0.463 (3)	0.477 (1)	5 (3)[a]
H162	−0.148 (3)	0.369 (3)	0.471 (1)	5 (3)[a]
H163	−0.176 (3)	0.484 (3)	0.450 (1)	5 (3)[a]
H21	0.170 (1)	0.342 (1)	0.1402 (6)	8 (3)[a]
H22	0.148 (1)	0.462 (1)	0.0784 (6)	8 (3)[a]
H24	0.157 (1)	0.690 (1)	0.1777 (6)	8 (3)[a]
H25	0.179 (1)	0.570 (1)	0.2395 (6)	8 (3)[a]
H261	0.127 (3)	0.627 (2)	0.055 (1)	5 (3)[a]
H262	0.198 (3)	0.700 (2)	0.091 (1)	5 (3)[a]
H263	0.071 (3)	0.709 (2)	0.093 (1)	5 (3)[a]
P	0.2500	0.2500	0.5190 (9)	3.8 (3)
F1	0.144 (2)	0.231 (3)	0.5221 (7)	14 (1)
F2	0.2500	0.2500	0.467 (1)	10 (1)
F3	0.2500	0.2500	0.574 (2)	7 (1)

[a] These atoms were refined isotropically. Anisotropically refined atoms are given in the form of the equivalent isotropic displacement parameter defined as $(4/3)[a^2\beta_{11} + b^2\beta_{22} + c^2\beta_{33} + ab(\cos\gamma)\beta_{12} + ac(\cos\beta)\beta_{13} + bc(\cos\alpha)\beta_{23}]$.

models in which the torsion angles were set to 0° to give D_{4h} symmetry.

The atomic coordinates used in the calculations in the D_4 symmetry were those from the crystal structure data for both compounds, except that the distances used for N–H and C–H are 1.06 and 1.08 Å, respectively. After modifying the system to the D_{4h} symmetry, the M–M and M–N distances were the same as before, but the other structure data were changed slightly. They are, for the Ni complexes, N–C = 1.284 Å, N–C–N = 125.0°, Ni–N–C = 120.6°, and Ni–Ni–N = 86.9°; and, for the Pd complexes, N–C = 1.264 Å, N–C–N = 127.6°, Pd–N–C = 115.7°, and Pd–Pd–N = 85.0°.

The starting molecular potential for the SCF procedure was obtained by superposition of Herman–Skillman atomic potentials in all calculations. The α values used for each atom were those of Schwarz.[18] For inter- and outer-sphere regions a valence electron weighted average of atomic α values was used. The atomic sphere radii were chosen as 88% of the atomic number radii[19] in the nickel compound in both symmetries, and 88.5% in D_4 symmetry and 89% in D_{4h} symmetry for the palladium compound. The atomic spheres were allowed to overlap. The outer-sphere radius was chosen tangential to the outermost atomic spheres. The spherical harmonics through l = 2, 1, and 0 were used in the metal, N, C, and H regions. In the outer-sphere region, l = 5 was used in the calculations in the D_{4h} symmetry, and l = 4 in the D_4 symmetry. The SCF calculations for both molecules in both symmetries were considered to be converged when the shift in potential was less than 0.001 Ryd.

The calculations on the $Ni_2(HNCHNH)_4^+$ and $Pd_2(HNCHNH)_4^+$ cations were done in a way similar to those for the neutral compounds in the D_4 symmetry. Because of the large torsional angle (27.35°) in the nickel cation, it did not seem pertinent to perform a calculation in D_{4h} symmetry. Atomic coordinates were therefore only those corresponding to the actual $[Ni_2(form)_4]^+$ and $[Pd_2(form)_4]^+$ structures but averaged to conform to strict D_4 symmetry.

(18) Schwarz, K. *Phys. Rev. B* **1972**, *5*, 2466; *Theor. Chim. Acta* **1974**, *34*, 225.
(19) Norman, J. G., Jr. *Mol. Phys.* **1976**, *31*, 1191.

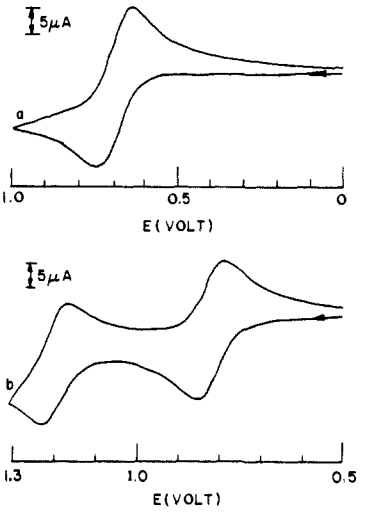

Figure 4. Cyclic voltammograms of $M_2(form)_4$ in CH_2Cl_2 (ca. 0.1 M n-Bu_4NPF_6) at a platinum electrode: (a) M = Ni; (b) M = Pd. Reference electrode: Ag/AgCl; scan speed = 200 mV·s^{-1}. The $FeCp_2$/$FeCp_2^+$ couple had $E_{1/2}$ = +0.49 V in the same conditions.

Results

Syntheses and Characterization. The neutral compounds $M_2(form)_4$ (M = Ni, Pd) were prepared by the reactions outlined in eq 1 and 2.

$$NiBr_2 + 2Li^+(form)^- \xrightarrow[\text{reflux}]{THF} {}^1/_2Ni_2(form)_4 + 2LiBr \quad (1)$$

$${}^1/_3Pd_3(OAc)_6 + 2Li^+(form)^- \xrightarrow[\text{ca. 25 °C}]{THF} {}^1/_2Pd_2(form)_4 + 2LiOAc \quad (2)$$

The nickel reaction required an excess of the lithium salt in order to obtain good yields, presumably because of the presence of water in the starting material.

A peculiar property of the products is their tendency to include interstitial solvent when crystallizing. By using several solvents, $Pd_2(form)_4$·2THF, $Pd_2(form)_4$·toluene, and $Pd_2(form)_4$·OEt_2 were obtained for the palladium compound. When the crystallization procedure was performed in air and in the CH_2Cl_2/n-hexane system, the water adducts, $M_2(form)_2$·$2H_2O$ (M = Ni, Pd), were obtained. The stoichiometry of the compounds with respect to the amount of solvent of crystallization was established by ^1H NMR spectrometry in each case.

The oxidation of the neutral $M_2(form)_4$ compounds was carried out both chemically and electrochemically. The cyclic voltammograms, shown in Figure 4, show a first reversible process for each compound [$E_{1/2}$ = +0.73 V (M = Ni), +0.81 V (M = Pd) vs a Ag/AgCl reference electrode] and a second process, which is reversible for Pd ($E_{1/2}$ = +1.19 V) but irreversible for Ni (E_{pc} = ca. +1.25 V). The two waves for each compound have the same limiting current and are therefore associated with the same number of electrons. Their monoelectronic nature was established by controlled-potential coulometry (carried out at +1.0 V for each compound), which generates the singly charged cations.

$$Ni_2(form)_4 \overset{E_{1/2} = +0.73\text{ V}}{\rightleftharpoons} [Ni_2(form)_4]^+ \xrightarrow{E_{pc} = +1.25\text{ V}} [Ni_2(form)_4]^{2+} \rightarrow \text{decomp} \quad (3)$$

$$Pd_2(form)_4 \overset{E_{1/2} = +0.81\text{ V}}{\rightleftharpoons} [Pd_2(form)_4]^+ \overset{E_{1/2} = +1.19\text{ V}}{\rightleftharpoons} [Pd_2(form)_4]^{2+} \quad (4)$$

The EPR spectra in CH_2Cl_2 glasses at liquid nitrogen temperature are displayed in Figure 1. The spectrum of the nickel species (Figure 1a) is indicative of axial symmetry, with $g_\perp$ = 2.210 and $g_\parallel$ = 2.038. The palladium compound, on the other

hand, shows only a symmetric line with $g = 2.014$. The visible/UV spectra of $[M_2(form)_4]^{n+}$ (M = Ni, Pd, $n = 0.1$) are reported in Figure 2.

A bulk electrolysis was attempted for the palladium species at +1.35 V in order to electrogenerate the $[Pd_2(form)_4]^{2+}$ species. More than two electrons per molecule were consumed in the process, and a control CV experiment showed that most of the electroactive species had been destroyed. Since the second oxidation process does not show any significant deviation from electroreversibility in the cyclic voltammogram (see Figure 4b), having $\Delta E_p = 55$ mV at a scan speed of 200 mV·s^{-1}, we attribute this behavior to a slow chemical process that follows the electrogeneration of $[Pd_2(form)_4]^{2+}$ and that presumably involves the formamidinato ligands. We have, in fact, theoretical evidence that the oxidation of the palladium species removes electrons from ligand-based orbitals (see Discussion).

The monocations, $[M_2(form)_4]^+$ (M = Ni, Pd), are stable to dry air in CH_2Cl_2 as solvent. When these solutions are left in contact with the laboratory atmosphere, however, they slowly generate the neutral dimers, $M_2(form)_4$, presumably because of involvement of moisture (eq 5).

$$[M_2(form)_4]^+ + {}^1/_2H_2O \rightarrow M_2(form)_4 + H^+ + {}^1/_4O_2 \quad (M = Ni, Pd) \quad (5)$$

The slight excess of charge consumed during the electrogeneration of $[Ni_2(form)_4]^+$ from $Ni_2(form)_4 \cdot 2H_2O$ (see Experimental Section) may perhaps also be so explained. Reduction to the neutral dimer was also observed when $[Pd_2(form)_4]^+$ interacted with dry MeCN or with n-Bu_4NBPh_4/CH_2Cl_2 during attempts to carry out ion metathesis reactions.

Chemical oxidation was achieved by using silver salts in dichloromethane as solvent. $Ni_2(form)_4$ was oxidized immediately and quantitatively to the monocation (as shown by visible spectroscopy) by $[Ag(MeCN)_x]BF_4$ (eq 6).

$$Ni_2(form)_4 + [Ag(MeCN)_x]BF_4 \xrightarrow{CH_2Cl_2} [Ni_2(form)_4]BF_4 + Ag + x\text{MeCN} \quad (6)$$

Crystals of the dinickel salt were obtained by diffusion of ether into the dichloromethane solution. An analogous reaction took place for the palladium compound, but subsequent ether diffusion yielded $Pd_2(form)_4 \cdot OEt_2$. The presence of acetonitrile and the greater oxidizing power of the palladium cation relative to that of the nickel cation may be responsible for the different behavior the two systems.

A salt of the dipalladium monocation was isolated from the solution obtained by oxidation with $AgPF_6$ (eq 7).

$$Pd_2(form)_4 + AgPF_6 \xrightarrow{CH_2Cl_2} [Pd_2(form)_4]PF_6 + Ag \quad (7)$$

IR spectroscopy for the two salts showed the presence of the fluoro anions. The BF_4^- anion in the nickel complex has a strong and broad band at 1100 cm^{-1}. This value is close to that found for the IR-active B–F stretching vibration of tetrahedral BF_4^- (T_d symmetry, 1070 cm^{-1}).[20] This indicates that the geometry of the BF_4^- ion is not severely distorted when it is packed in the $[Ni_2(form)_4]^+$ salt and is in agreement with the results of the crystal structure determination, which imply loose packing. The PF_6^- ion in the dipalladium salt, on the other hand, appears to be significantly perturbed by its crystal environment. It exhibits a strong band at 1160 cm^{-1}, whereas the T_{1u}-symmetry stretching vibration for the octahedral ion is found at 840 cm^{-1}.[21] The crystal structure determination (vide infra) shows that the PF_6^- ion is lying on a crystallographic fourfold axis midway between two $[Pd_2(form)_4]^+$ ions, and the symmetry is therefore reduced from O_h to D_{4h}. The T_{1u} vibration, as a consequence, splits into two IR-active vibrations, $A_{2u} + E_u$. The energy of the E_u vibration, in which the four P–F bonds perpendicular to the fourfold axis participate, should not be strongly affected by the interaction with the dipalladium cations, but for the A_{2u} vibration, close contact with the cations might well increase the effective force constant. We suggest, therefore, that the band observed at 1160 cm^{-1} is due to the A_{2u} stretching mode, the energy increase with respect to the T_{1u} band of the octahedral PF_6^- being due to the axial interaction with the palladium centers. A sharp band observed at 850 cm^{-1} for $[Pd_2(form)_4]PF_6$, but not present in the IR spectrum of the parent neutral dimer, might be assigned to the E_u mode. Another IR-active T_{1u} mode[21] for octahedral PF_6^- at 555 cm^{-1}, due to a P–F bending mode, should also split into two IR-active A_{2u} and E_u modes in D_{4h} symmetry, and a fifth band (E_u) should arise from an IR and Raman inactive T_{2u} mode (calculated at 402 cm^{-1}),[21] but the assignment of these bands is very problematical because of their weakness and extensive overlapping with bands of the $[Pd_2(form)_4]^+$ ion that appear in the same region of the spectrum.

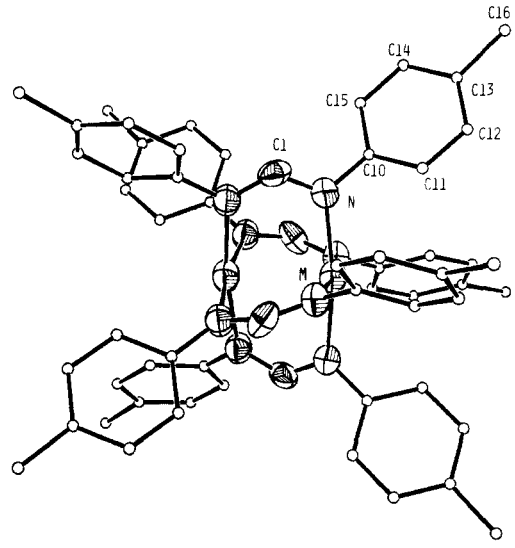

Figure 5. ORTEP view of the $M_2(form)_4$ (M = Ni, Pd) molecules in $M_2(form)_4 \cdot 2H_2O$.

The IR spectrum of the palladium salt, $[Pd_2(form)_4]PF_6$, also shows a very broad and strong band in the 4000–1700-cm^{-1} region, with a maximum around 2500 cm^{-1}. This does not have the appearance of a vibrational band and may possibly be attributed to a low-lying electronic transition.

The chemical oxidation of $Pd_2(form)_4$ with Cl_2 was attempted. No reaction took place in CCl_4 as solvent under either thermal or photochemical conditions or a combination of both. In CH_2Cl_2, a change of color was observed at room temperature, but this did not persist and only the starting material was recovered.

Crystal Structures. The $M_2(form)_4 \cdot 2H_2O$ (M = Ni, Pd) compounds crystallize in the cubic space group $Pn\bar{3}n$, with the dimers occupying 42 special positions (i.e., they have imposed D_4 symmetry). The two metal atoms in each compound are bridged by four formamidinato ligands, with four nitrogen atoms around each metal atom in a square-planar configuration. A view of the molecule, valid for both metals, is shown in Figure 5. The most interesting feature is the metal–metal separation, which is 2.485 (2) Å for M = Ni and 2.622 (3) Å for M = Pd. These distances compare with those in other dimers of similar configuration [e.g., for Ni: 2.395 (3) Å in $Ni_2(N_3Ph_2)_4$,[5] 2.551 (3) Å in $Ni_2(S_2CCH_2Ph)_4$,[6] and 2.564 (1) Å in $Ni_2(S_2CCH_3)_4$;[22] for Pd: 2.5626 (7) Å in $Pd_2(N_3Ph_2)_4$,[5] 2.715 (3) Å in $Pd_2(S_2CCH_2Ph)_4$,[6] 2.754 (1) and 2.738 (1) Å in form A and form B of $Pd_2(S_2CCH_3)_4$,[23] 2.546 (1) Å in $Pd_2(mhp)_4$ (mhp = 6-methylhydroxypyridinato),[4] 2.745 (1) Å in $Pd_2(bttz)_4$ (bttz = μ-1,3-benzothiazole-2-thiolato-N,S),[24] 2.547–2.570 Å in a series of $Pd_2(xhp)_4$

(20) Quist, A. S.; Bates, J. B.; Boyd, G. E. *J. Chem. Phys.* **1971**, *54*, 4896.
(21) Mayfield, H. G.; Bull, W. E. *J. Chem. Soc. A* **1971**, 2280.
(22) Bellitto, C.; Dessy, G.; Fares, V. *Inorg. Chem.* **1985**, *24*, 2815.
(23) Piovesana, O.; Bellitto, C.; Flamini, A.; Zanazzi, P. F. *Inorg. Chem.* **1979**, *18*, 2258.
(24) Kubiak, M. *Acta Crystallogr., Sect. C* **1985**, *C41*, 1288.

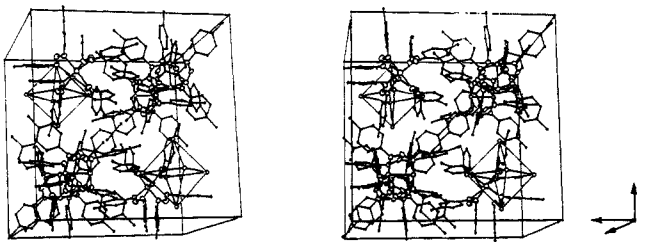

Figure 6. Stereoview of the unit cell for compounds $M_2(form)_4 \cdot 2H_2O$ (M = Ni, Pd).

compounds (xhp = 6-X-hydroxypyridinato, X = Cl, CH_3),[25] and 2.677 (1) Å in $Pd_2(pyt)_4$ (pyt = pyridine-2-thiolato).[26] To our knowledge, only the triazenato compounds, $M_2(N_3Ph_2)_4$ (M = Ni, Pd),[5] for both nickel and palladium, have shorter metal–metal separations than those in the formamidine dimers. Other relevant bond distances and angles are reported in Table IV.

The unit cells of $M_2(form)_4 \cdot 2H_2O$ (M = Ni, Pd) contain six dinuclear units arranged so as to leave a considerable amount of empty volume around the crystallographic 432 positions (two in the unit cell). Each of these is filled in with six water molecules. The oxygen atoms reside on the fourfold axes and define a perfect octahedron. A stereoview of the packing in the unit cell is shown in Figure 6. The thermal motion of the oxygen atoms is very high, and the M···O and O···O contacts are >5 Å in all cases. The O···O contact in hydrogen-bonded ice is around 2.75 Å.[27] This very unorthodox arrangement is presumably the result of a competition between the tendency of the oxygen atoms to cluster together via formation of hydrogen bonds (energy drive) and their tendency to fully occupy the large volume of the cavity (entropy drive), with the latter being dominant. The required symmetry for the $(H_2O)_6$ cluster is also working against the energy drive, since the most stable form of ice is one containing tetrahedrally packed oxygen atoms.[28] In order to see what the effect of lowering the temperature would be on the energy–entropy balance, we redetermined the structure of the nickel compound at a lower temperature (−105 °C). The only major effect was a reduction of the thermal motion of the water oxygen atom, whereas its position does not substantially change. The other parameters are also very similar to those of the room-temperature structure (see Table IV). Figure 3 shows a contour map of the electron density in the region occupied by the water molecules, obtained from a difference Fourier map at the end of the refinement for the $Pd_2(form)_4$ molecule.

The structure of the $[M_2(form)_4]^+$ ions (M = Ni, Pd) is similar to that of the corresponding neutral complexes, although the cations have lower crystalographically imposed symmetry (C_4). The anions (BF_4^- for the nickel structure and PF_6^- for the palladium structure) reside on the fourfold axes which are common to the cations, with average contacts Ni···F = 4.349 [3] Å and Pd···F = 4.41 [5] Å. The ions are therefore packed along the *c* axis so as to give an alternation of cations and anions. A drawing of this arrangement of the ions along the axis for $[Pd_2(form)_4]PF_6$ is shown in Figure 7. Figures 8 and 9 show stereoviews of the unit cells for compounds $[Ni_2(form)_4]BF_4$ and $[Pd(form)_4]PF_6$, respectively.

The metal–metal distance in $[Ni_2(form)_4]^+$ is 2.418 (4) Å, i.e., 0.067 (4) Å *shorter* than that found for the corresponding neutral complex, while the M–M distance in $[Pd_2(form)_4]^+$ is 2.637 (6) Å, i.e., 0.015 (6) Å *longer* than that found for the corresponding neutral complex. A tentative explanation of this effect is given in the Discussion. While no $[Pd_2(X-X)_4]^+$ (X–X = bridging monoanionic ligand) structure has been reported (indeed, no

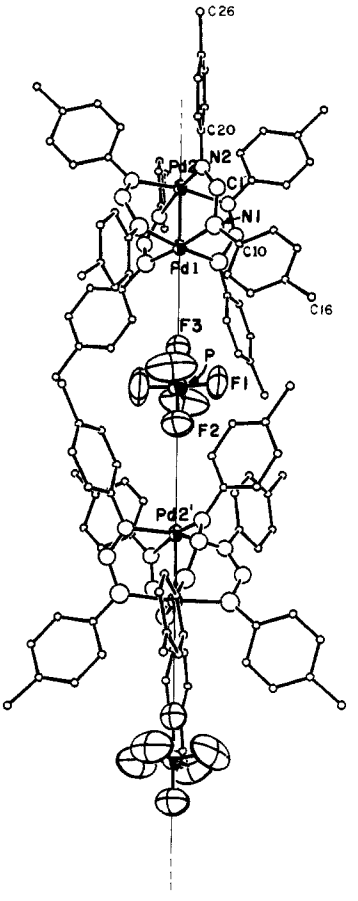

Figure 7. Packing of $[Pd_2(form)_4]PF_6$ along the *c* axis.

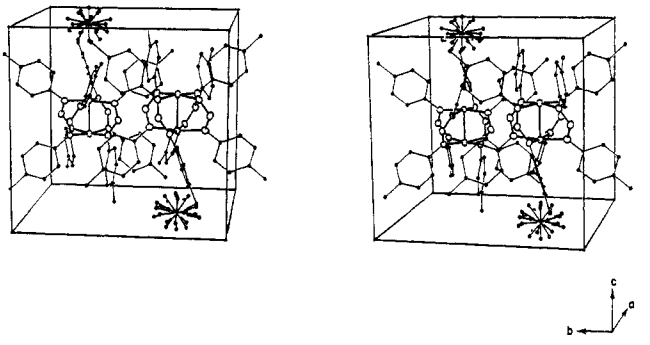

Figure 8. Stereoview of the unit cell for compound $[Ni_2(form)_4]BF_4$.

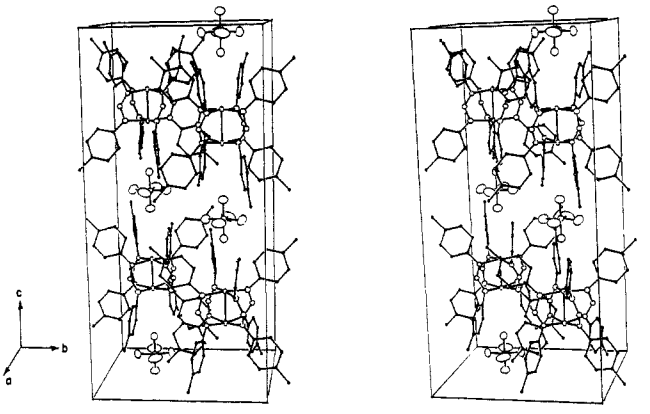

Figure 9. Stereoview of the unit cell for compound $[Pd_2(form)_4]PF_6$.

compound containing such an ion seems to have ever been prepared), a $[Ni_2(X-X)_4]^+$ structure is known for (X–X) = S_2CCH_3,[22] which shows a metal–metal distance of 2.514 (5) Å. This is 0.050 (5) Å shorter than that found for the corresponding

(25) Bancroft, D. P.; Cotton, F. A.; Falvello, L. R.; Schwotzer, W. *Inorg. Chem.* **1986**, *25*, 1015.
(26) Umakoshi, K.; Kinochita, I.; Ooi, S. *Inorg. Chim. Acta* **1987**, *127*, L41.
(27) Cotton, F. A.; Wilkinson, G. *Advanced Inorganic Chemistry*, 4th ed.; Wiley: New York, 1980; p 224.
(28) Krindel, P.; Eliezer, I. *Coord. Chem. Rev.* **1971**, *3*, 217.

Table VIII. Upper Occupied Molecular Orbitals for $Ni_2(HNCHNH)_4$ in D_{4h} and D_4 Symmetries[a]

D_{4h} level	energy	% charge 2 Ni	8 N	4 C	4 H	8 H	Ni angular contribution			D_4 level	energy	% charge 2 Ni	8 N	4 C	4 H	8 H	Ni angular contribution		
$1a_{1u}$	−5.251	0	100	0	0	0			100% d_{xy}	$6b_1$	−5.664	58	42	0	1	0			100% d_{xy}
$2b_{1u}$	−5.313	65	35	0	0	0			100% d_{xy}	$6a_1$	−5.911	2	97	0	1	0			
$4a_{2u}$	−5.963	96	3	0	0	1	5% s	1% p	94% d_{z^2}	11e	−6.167	14	84	1	1	0		2% p	98% $d_{xz,yz}$
$5e_g$	−6.038	2	98	0	0	0				$5a_2$	−6.325	94	5	0	0	1	5% s	1% p	94% d_{z^2}
$2b_{2g}$	−6.547	91	3	6	0	0			100% d_{xy}	$5b_2$	−6.924	89	4	7	0	0			100% d_{xy}
$4e_g$	−6.638	97	2	0	0	1			100% $d_{xz,yz}$	10e	−7.030	96	2	1	0	1			100% $d_{xz,yz}$
$6e_u$	−7.039	94	4	0	0	2			100% $d_{xz,yz}$	9e	−7.641	89	9	1	0	1			100% $d_{xz,yz}$
$5a_{1g}$	−7.585	98	2	0	0	0	9% s	1% p	90% d_{z^2}	$5a_1$	−7.966	97	1	1	1	0	10% s		90% d_{z^2}
$5e_u$	−8.056	13	56	14	12	5		66% p	34% $d_{xz,yz}$	8e	−8.362	10	62	15	8	5		77% p	23% $d_{xz,yz}$
$1b_{1u}$	−8.574	55	45	0	0	0			100% d_{xy}	$4a_2$	−8.658	2	65	33	0	0			
$1a_{2g}$	−8.822	0	65	35	0	0				$5b_1$	−8.683	60	40	0	0	0			100% d_{xy}
$4b_{1g}$	−9.792	42	30	10	13	5			100% $d_{x^2-y^2}$	7e	−9.618	11	64	14	5	5		70% p	30% $d_{xz,yz}$
$4e_u$	−9.851	4	62	28	5	1				$4b_1$	−10.314	42	32	10	12	4			100% $d_{x^2-y^2}$
$3e_g$	−9.973	13	73	1	0	13		93% p	7% $d_{xz,yz}$	$4b_2$	−10.489	21	58	17	0	4			100% d_{xy}
$4a_{1g}$	−10.133	21	35	16	21	7	60% s		40% d_{z^2}	6e	−10.519	10	71	10	1	8		98% p	2% $d_{xz,yz}$
$1b_{2g}$	−10.800	16	61	23	0	0			100% d_{xy}	$4a_1$	−10.608	22	37	16	19	6	57% s		43% d_{z^2}
$3b_{2u}$	−11.080	36	50	0	0	14			100% $d_{x^2-y^2}$	$3b_2$	−11.693	37	51	4	0	8			100% $d_{x^2-y^2}$
$3a_{2u}$	−11.691	21	58	0	0	21	52% s		48% d_{z^2}	$3a_2$	−12.181	22	58	1	0	19	53% s		47% d_{z^2}

[a] Here and in Tables IX and X energies are in eV, % charge means relative amount of charge in the two M spheres, eight N spheres, etc., and metal angular contribution is given only when >10%.

Table IX. Upper Occupied Molecular Orbitals for $Pd_2(HNCHNH)_4$ in D_{4h} and D_4 Symmetries

D_{4h} level	energy	% charge 2 Pd	8 N	4 C	4 H	8 H	Pd angular contribution			D_4 level	energy	% charge 2 Pd	8 N	4 C	4 H	8 H	Pd angular contribution		
$1a_{1u}$	−6.006	0	100	0	0	0			100% d_{xy}	$6b_1$	−6.198	35	65	0	0	0			100% d_{xy}
$2b_{1u}$	−6.051	38	62	0	0	0			100% d_{xy}	$6a_1$	−6.371	1	98	0	1	0			
$5e_g$	−6.584	0	100	0	0	0				11e	−6.530	6	90	1	3	0			
$4a_{2u}$	−6.896	86	12	0	0	2	8% s	1% p	91% d_{z^2}	$5a_2$	−6.916	82	15	1	0	2	8% s	1% p	91% d_{z^2}
$6e_u$	−7.784	17	54	9	12	8		46% p	54% $d_{xz,yz}$	10e	−7.980	15	62	8	8	7		38% p	62% $d_{xz,yz}$
$2b_{2g}$	−8.160	78	11	11	0	0			100% d_{xy}	$5b_2$	−8.234	75	13	12	0	0			100% d_{xy}
$4e_g$	−8.362	91	6	0	0	3		1% p	99% $d_{xz,yz}$	9e	−8.390	72	20	2	1	5		4% p	96% $d_{xz,yz}$
$5a_{1g}$	−8.846	56	23	8	10	3	39% s	2% p	59% d_{z^2}	$5a_1$	−8.810	55	26	7	9	3	36% s	2% p	62% d_{z^2}
$5e_u$	−9.319	85	8	5	2	0			100% $d_{xz,yz}$	$4a_2$	−9.238	5	65	30	0	0			
$1a_{2g}$	−9.602	0	67	33	0	0				8e	−9.322	74	20	5	0	1			100% $d_{xz,yz}$
$1b_{1u}$	−9.907	77	23	0	0	0			100% d_{xy}	7e	−9.704	50	40	5	2	3		7% p	93% $d_{xz,yz}$
$3e_g$	−9.967	19	70	1	0	10		43% p	57% $d_{xz,yz}$	$5b_1$	−9.849	79	20	0	1	0			100% d_{xy}
$4e_u$	−10.281	7	61	29	2	0				6e	−10.415	7	68	21	1	3			
$4a_{1g}$	−10.553	62	15	8	11	4	1% s		99% d_{z^2}	$4a_1$	−10.712	61	17	8	10	4			100% d_{z^2}
$4b_{1g}$	−10.786	44	19	14	18	5			100% $d_{x^2-y^2}$	$4b_1$	−11.015	45	22	13	16	4			100% $d_{x^2-y^2}$
$1b_{2g}$	−11.470	33	50	17	0	0			100% d_{xy}	$4b_2$	−11.040	37	46	13	0	4			100% d_{xy}
$3a_{2u}$	−11.861	30	53	0	0	17	26% s	1% p	73% d_{z^2}	$3a_2$	−11.936	30	54	2	0	14	24% s		76% d_{z^2}
$3b_{2u}$	−12.222	40	45	0	0	15			100% $d_{x^2-y^2}$	$3b_2$	−12.471	41	45	3	0	11			100% $d_{x^2-y^2}$

neutral complex.[22] However, this system differs from ours in that a strong axial interaction exists between the nickel atoms and iodide atoms that bridge two of the nickel dimers (Ni–I = 2.935 [4] Å).[22]

In addition to the shortened M–M distance on going from $Ni_2(form)_4$ to $[Ni_2(form)_4]^+$, the twist angle (i.e., the N(1)–Ni(1)–Ni(2)–N(2) torsion angle) increases from 16.8 (3) to 27.4 (4)°. In the palladium system, on the other hand, the slight lengthening of the metal–metal bond is accompanied not by a decrease but rather by a small increase of the N(1)–Pd(1)–Pd(2)–N(2) torsion angle [from 15.1 (6) to 17.0 (1)°]. This change is, however, hardly significant because of the high esd values.

An interesting aspect of the $[Ni_2(form)_4]^+$ structure is that the packing of the cations determines the symmetry of the space group and the small BF_4^- anions are therefore forced to be disordered on crystallographic fourfold axes (a problem that does not exist for the PF_6^- anions in the palladium structure). As a result, the BF_4^- anion does not have preferential interactions with the neighboring nickel atoms. The PF_6^- ion, on the contrary, has axial interactions with the palladium atoms and these influence its vibrational properties, as discussed above. We note that the tetrahedral BF_4^- ion could have been accommodated in an ordered fashion in the same space group on the $\bar{4}$ positions. The reason this does not occur is presumably that a great deal of van der Waals interaction between the phenyl groups of dimers on adjacent axes would be lost if those axes were further separated by increasing the *a* and *b* dimensions of the cell in order to create room for BF_4^-. The placement of BF_4^- on the fourfold axes in the cavities between dimers, on the other hand, does not severely interfere with the packing of the structure (see Figure 8), and is at least as favorable electrostatically.

Electronic Structures

$M_2(HNCHNH)_4$ Molecules. The results of the SCF–Xα–SW calculations for the nickel and palladium systems are summarized in Tables VIII and IX, respectively, which describe the upper filled orbitals, ranging from ca. −12 to −5 eV. In each case there are also 20 lower-lying filled valence MOs (−26.3 to −13.9 eV for the nickel compound and −27.3 to −14.8 eV for the palladium compound) that are essentially unperturbed ligand orbitals responsible for N–C, N–H, and C–H σ bonds. These require no discussion here. The levels listed in Tables VIII and IX contain 24 electron pairs and are responsible for N–C π-bonding, metal–ligand bonding, metal–metal bonding, and metal–metal antibonding interactions.

The calculated Xα total energy for the Ni compound is −7223.3 and −7222.6 Ryd, and the virial-theorem ratio $-2T/V$ is 1.000086 and 1.000140 in the D_{4h} and D_4 symmetry, respectively. For the Pd compound the results in the two symmetries are E = −20948.2 and −20947.0 Ryd and $-2T/V$ = 0.999962 and 1.000052, respectively. The ionization potentials for the Ni and Pd compounds in D_4 symmetry are 7.89 and 8.40 V, respectively.

In Tables VIII and IX both D_{4h} and D_4 levels are given, together with their energies, relative charge distribution within the atomic spheres, and the metal angular contributions for levels with more than 10% metal character. The two members of the pairs of correlated orbitals are very similar in energy and character. The only notable differences from one symmetry to the other are the reversal of order for a few pairs of orbitals, an example being the highest pair of orbitals. Since the $1a_{1u}/6a_1$ orbital is entirely a

Table X. Upper Occupied Molecular Orbitals for the $[M_2(HNCHNH)_4]^+$ Ions with M = Ni and Pd

$Ni_2(N_2H_2CH)_4^+$										$Pod_2(N_2H_2CH)_4^+$									
D_4		% charge					Ni angular contribution			D_4		% charge					Pd angular contribution		
level	energy	2 N	8 N	4 C	4 H	8 H				level	energy	2 Pd	8 N	4 C	4 H	8 H			
$6b_1$	−10.04	42	57	0	1	0			100% d_{xy}	$6b_1$	−10.45	30	70	0	0	0			100% d_{xy}
11e	−10.23	14	83	1	2	0			100% $d_{xz,yz}$	$6a_1$	−10.59	1	98	0	1	0			
$6a_1$	−10.55	3	94	1	1	1				11e	−10.78	4	93	1	2	0			
$5a_2$	−10.76	89	9	1	0	1	6% s	1% p	93% d_{z^2}	$5a_2$	−11.39	78	18	2	0	2	8% s	1% p	91% d_{z^2}
$5b_2$	−11.51	88	6	6	0	0			100% d_{xy}	10e	−12.21	12	64	9	9	6		55% p	45% $d_{xz,yz}$
10e	−11.56	89	7	3	0	1			100% $d_{xz,yz}$	$5b_2$	−12.60	68	18	14	0	0			100% d_{xy}
9e	−12.29	78	15	5	2	0			100% $d_{xz,yz}$	9e	−12.83	65	26	3	1	5		4% p	96% $d_{xz,yz}$
8e	−12.43	25	58	7	5	5		27% p	73% $d_{xz,yz}$	$5a_1$	−13.10	51	28	8	10	3	39% s	1% p	60% d_{z^2}
$4a_2$	−12.54	9	63	28	0	0				$4a_2$	−13.32	5	65	30	0	0			
$5a_1$	−12.64	95	3	1	1	0	11% s	1% p	88% d_{z^2}	8e	−13.77	70	22	7	0	1			100% $d_{xz,yz}$
$5b_1$	−12.72	74	25	1	0	0			100% d_{xy}	7e	−14.18	59	32	5	2	2		5% p	95% $d_{xz,yz}$
7e	−13.43	19	60	11	5	5		41% p	59% $d_{xz,yz}$	$5b_1$	−14.35	82	18	0	0	0			100% d_{xy}
$4b_2$	−14.32	24	58	15	0	5			100% d_{xy}	6e	−14.50	14	64	17	1	4		32% p	68% $d_{xz,yz}$
$4b_1$	−14.46	46	30	10	10	4			100% $d_{x^2-y^2}$	$4a_1$	−15.17	63	15	8	10	4			100% d_{z^2}
$4a_1$	−14.61	25	38	15	16	6	48% s		52% d_{z^2}	$4b_2$	−15.34	44	42	11	0	3			100% d_{xy}
6e	−14.63	9	70	14	1	6				$4b_1$	−15.45	44	20	15	17	4			100% $d_{x^2-y^2}$
$3b_2$	−15.85	40	49	5	0	6			100% $d_{x^2-y^2}$	$3a_2$	−16.29	32	52	1	0	15	21% s		79% d_{z^2}
$3a_2$	−16.20	24	57	3	0	16	50% s		50% d_{z^2}	$3b_2$	−16.87	42	44	1	0	13			100% $d_{x^2-y^2}$

nitrogen lone pair orbital, it has no direct effect on M–M bonding and its exact position is not for the moment critical. None of the other reversals are of any significance. In the following discussions of the neutral molecules we shall refer specifically to the orbitals according to their labels in D_{4h} symmetry.

Let us turn first to the neutral dinickel molecule (Table VIII). A few of the orbitals are essentially pure ligand π or lone pair orbitals, viz., $1a_{1u}$, $1a_{2g}$ (which have no symmetry match whatsoever with metal atomic orbitals) and the $4e_u$, $5e_g$ which show only miniscule metal character, even though this would not be forbidden by symmetry. Another set of molecular orbitals that we can identify as a group are those responsible for the set of metal–ligand σ bonds. Purely on the basis of symmetry arguments we can anticipate which representations MOs which serve this function must belong to, and inspection of Table VIII reveals the following appropriate set: $4a_{1g}$, $4b_{1g}$, $3a_{2u}$, $3b_{2u}$, $3e_g$, $5e_u$. In all of these the metal character is low but appreciable (13–42%) while the ligand character is higher, in accord with the expected Ni^+–N^- bond polarity.

Having disposed of these orbitals, whose character is fairly easy to recognize, and which play little or no role in metal–metal bonding, we can now turn to the remaining occupied orbitals listed in Table VIII. Six of them have high (65–98%) metal character. These orbitals may be regarded, to a good approximation, as bonding and antibonding combinations of metal d orbitals. We have as σ and σ^* the $5a_{1g}$ and $4a_{2u}$ orbitals; as π and π^* the $6e_u$ and $4e_g$ orbitals; and as δ and δ^* the $2b_{2g}$ and $2b_{1u}$ orbitals.

The two remaining orbitals are $1b_{2g}$ (with 16% metal content) and $1b_{1u}$ (with 55% metal content), which have δ and δ^* characters, respectively. While these, especially the latter, may be considered as members of the Ni–Ni manifold, they may also, and perhaps more appropriately, be considered to represent metal–ligand bonding of the type that results from overlap of the ligand π system with the d_{xy} orbitals of the metal atoms. It is this pair of strong metal–ligand type δ interactions that may be considered responsible for raising the energies of both the δ and δ^* orbitals of mainly Ni–Ni type to higher energies than the π^* ($4e_g$) orbital, and indeed into the energy region of the σ^* ($4a_{2u}$) orbital.

At this point we can address the question of whether there is any reason to believe in the existence of direct bonding (of order <1, of course) between the nickel atoms or whether their relatively close approach should be attributed entirely to the clamping effect of the four formamidinato ligands. Obviously, on the basis on a "zero-ith order" analysis, we must conclude that there is no Ni–Ni bond, since all conjugate pairs of bonding and antibonding MOs are filled equally. However, as inspection of Table VIII (and, similarly, Table IX) shows, there is appreciable participation of metal *n*s and *n*p orbitals (n = 4 for Ni, 5 for Pd) in the molecular orbitals. This *n*s and *n*p participation is greater here than in other cases where the metal atoms are from earlier groups, i.e., $Cr_2(O_2CH)_4$,[29] $Mo_2(O_2CH)_4$,[30] and $Rh_2(O_2CH)_4$.[31] In an indirect way, the introduction of this *n*s and *n*p character into the mainly metal–ligand bonding MOs may allow some enhancement of the metal–metal interactions carried by the metal d orbitals.

Turning now to the neutral dipalladium compound, we see that the results in Table IX are generally similar to those for the nickel analogue. The principal differences are reversals of the *n*s and *n*p contributions for the $4a_{1g}/5a_{1g}$ and $5e_u/6e_u$ pairs, respectively. For the palladium compounds the σ, π, and δ bonding roles are played by the $4a_{1g}$, $5e_u$, and $2b_{2g}$ MOs; their antibonding counterparts, however, remain the same as in the nickel case, although the $2b_{1u}$ orbital now has less metal content. Conversely, it is now the $5a_{1g}$ and $6e_u$ MOs that have the most significant *n*s and *n*p character.

Finally, we consider the results of the calculations for the cations, $[M_2(form)_4]^+$, which are presented for both cases in Table X for D_4 symmetry. For both compounds we see that the half-occupied orbital is the $6b_1$ orbital. However, for several reasons, we must view this result with caution. Considering the results for the cations themselves, we see that immediately below these $6b_1$ orbitals (which have appreciable metal character) are two orbitals that are mainly ligand based. It is not at all unlikely that the calculation could give an incorrect order for such closely spaced orbitals that have such diverse provenances. It is also pertinent to recall that for the neutral molecules the ordering of the two highest filled orbitals showed a dependence on the angle of torsion about the M–M axis, which is another cautionary sign that this ordering is a sensitive function of the computational parameters. We shall return to this point in discussing the structural and EPR results for the cations.

As for the remaining MOs of the cations, they map into those of the corresponding neutral compounds rather directly, as would be expected. There are numerous changes in the energy ordering and some shifts in atomic orbital provenances, but there is no major change in the overall electronic structures.

Discussion

We shall now examine the experimental and theoretical results to see how well they advance our objective of better understanding the d^8–d^8 dinuclear molecules of type I. The formamidinato ligand, like the triazinato ligand, appears to have the capacity to promote the formation of such dinuclear species and enhance their ability to undergo reversible oxidation. The formamidinato ligand can

(29) Cotton, F. A.; Stanley, G. G. *Inorg. Chem.* **1977**, *16*, 2668.
(30) Norman, J. G., Jr.; Kolari, H. J.; Gray, H. B.; Trogler, W. C. *Inorg. Chem.* **1977**, *16*, 987.
(31) Norman, J. G., Jr.; Kolari, H. J. *J. Am. Chem. Soc.* **1978**, *100*, 791.

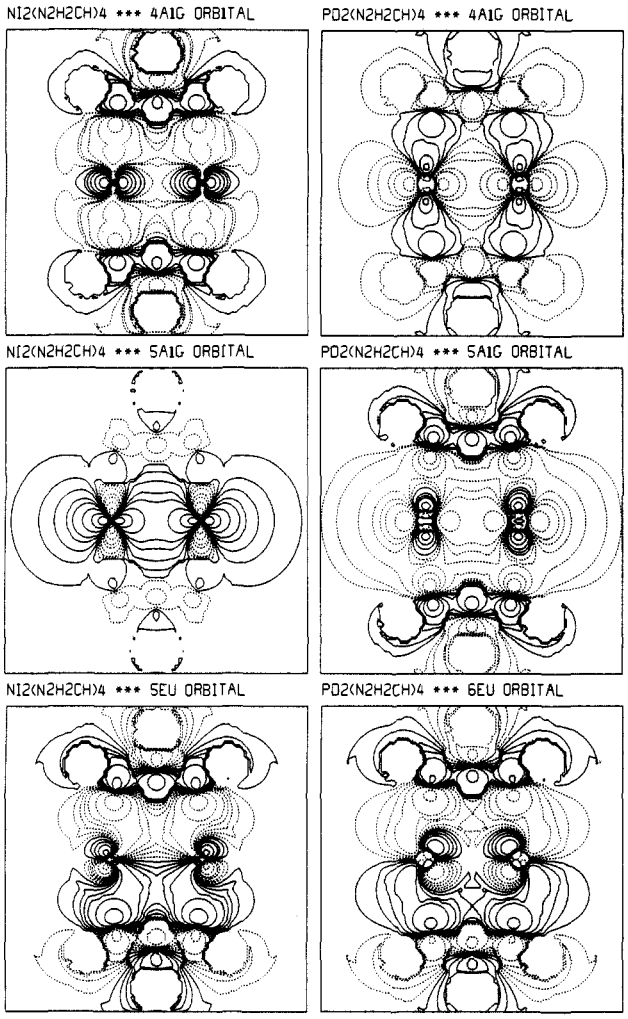

Figure 10. Contour plots of the $4a_{1g}$, $5a_{1g}$, and $5e_u$ orbitals of $Ni_2(HNCHNH)_4$ and the $4a_{1g}$, $5a_{1g}$, and $6e_u$ orbitals of $Pd_2(HNCHNH)_4$, with solid lines for positive regions and broken lines for negative regions of the wave functions.

also be modeled for purposes of molecular orbital calculations quite satisfactorily as an $HNCHNH^-$ ion.

By employing the structural results obtained for the $M_2(form)_4$ molecules as input for $X\alpha$ calculations on the model $M_2(HNCHNC)_4$ systems, we have obtained a description of the ground-state electronic structures of these molecules. The general conclusion to be drawn from these results is that, despite the rather short Ni–Ni (ca. 2.49 Å) and Pd–Pd (ca. 2.62 Å) distances, the "zero-ith order" prediction that no metal–metal bonding occurs is essentially correct.

One conclusion that is completely unambiguous is that no pair of *n*s or *n*p orbitals, in either molecule, overlap in such a way as to provide a separate, additional M–M bonding orbital that can be filled at the expense of a d-orbital-based antibonding orbital, thus affording a net, direct increase in the M–M bond order. While this might have been considered in advance as a possibility, the calculations show that it does not happen.

The *n*s and *n*p metal valence shell orbitals participate in ways that cannot be simply described, and which are somewhat different for the nickel and palladium compounds. The contour diagrams in Figure 10 (as well as others which are not shown because of space limitations) can be used to supplement the numerical results given in Tables VIII and IX in understanding the roles played by the various MOs in bonding. For $Ni_2(HNCHNH)_4$, the 4s orbital contributes to the $3a_{2u}$, $4a_{1g}$, $5a_{1g}$, and $4a_{2u}$ MOs to about the same extent, namely, 5–12%. The $3a_{2u}$ and $4a_{1g}$ MOs are mainly involved in Ni–N bonding as can be seen for the $4a_{1g}$ orbital in Figure 10. The $5a_{1g}$ orbital, which is about 87% nickel d_{z^2} and 9% nickel 4s is almost entirely responsible for Ni–Ni σ bonding. Its antibonding counterpart, the $4a_{2u}$ orbital, has about half as much 4s character, which may result in the σ bonding interaction slightly outweighing the σ antibonding. The nickel p orbitals contribute significantly only to the $3e_g$ and $5e_u$ orbitals and both of these are mainly concerned with Ni–N bonding, as can be seen in Figure 10 for the $5e_u$ orbital. It is the $6e_u$ and $4e_g$ orbitals, to which the 4p orbitals make no contribution, that are responsible for the offsetting π and π^* interactions between the metal atoms.

For $Pd_2(HNCHNH)_4$, the metal 5s orbitals contribute significantly to only three MOs: $3a_{2u}$ (which, as in the Ni case, is involved mainly with Pd–N bonding), $5a_{1g}$ and $4a_{2u}$ (which again is predominantly Pd–Pd σ^* in character). It can be seen from Figure 10 that the $4a_{1g}$ orbital in the Pd compound is the principal source of Pd–Pd σ bonding (in contrast to the Ni case), but it also has some Pd–N bonding character. Again, however, the $5a_{1g}$ orbital contributes to metal–metal σ bonding. The palladium 5p contributions are to the $3e_g$ (as in the nickel case) and $6e_u$ (in contrast to the nickel case) MOs. Again, the $3e_g$ orbital plays mainly the role of Pd–N bonding, but now it is the $6e_u$ orbital which is Pd–N bonding and the $5e_u$ orbital which supplied the Pd–Pd π bonding. The $4e_g$ MO again is the metal–metal π^* orbital. The role reversal for the $5e_u$ and $6e_u$ orbitals from the Ni to the Pd compound is also accompanied by their changing positions relative to the $4e_g(\pi^*)$ orbital.

We finally turn to the cations, $[M_2(form)_4]^+$. In the nickel case, the EPR spectrum shows $g_\parallel$ and $g_\perp$ values that indicate an orbital with considerable metal character for the odd electron. This is consistent with the MO calculation, which places the odd electron in the $6b_1$ orbital, which has 42% metal d_{xy} character. Since this orbital is also somewhat antibonding (δ^*, in a Ni–Ni sense) we have an explanation for the modest decrease (ca., 0.07 Å) in the Ni–Ni distance on going from $Ni_2(form)_4$ to $[Ni_2(form)_4]^+$. In the palladium case, the EPR spectrum indicates that the odd electron is in a ligand-based orbital, and the occurrence of only a slight change (+0.015 Å) in the Pd–Pd distance on ionization also implies that the electron was removed from a nonbonding orbital in the Pd–Pd sense. While the MO calculation, taken at face value, suggests for $[Pd_2(form)_4]^+$ as well as for the nickel compound that the hole should be in the $6b_1$ orbital (which is not consistent with the experimental data), it must be noted that there are two ligand-based orbitals ($6a_1$ and $11e$) that are very similar in energy to the $6b_1$ orbital. It would not be surprising if the calculated energies are slightly in error so that the odd electron can be assigned to one of these ligand-based orbitals.

A practical conclusion that emerges from this study is that it is apparently not possible to prepare a genuine Pd_2^{5+} complex (oxidation of the Pd_2^{4+} species having been found to occur on the ligand rather than the metal), and it thus seems entirely unlikely that any Pd_2^{6+} complex will be accessible. This is consistent with our observation that $Pd_2(form)_4$ is resistant to oxidation by Cl_2. In short, while there are a great many, and varied, Rh_2^{4+} compounds, a moderate number of (isoelectronic) Pt_2^{6+} compounds, and at least one Ir_2^{4+} compound, the prospects for any authentic Pd_2^{6+} compound appear very dim.

In closing we also remind the reader of the very strong and broad near-IR absorption band observed for $Pd_2(form)_4PF_6$. This rather anomalous spectral feature invites further study, but that must await improvements in the preparative procedures so that larger homogeneous samples of the pure compound can be obtained.

Acknowledgment. We are grateful to the National Science Foundation for support of this work and to Dr. Larry R. Falvello for crystallographic advice.

Supplementary Material Available: Full lists of bond distances, bond angles, and anisotropic displacement parameters for **1**·2H_2O (20 °C), **1**·2H_2O (−105 °C), **2**·2H_2O, **3**, and **4**, and fractional atomic coordinates and isotropic displacement parameters for **2**·OEt_2 (18 pages); observed and calculated structure factors for **1**·2H_2O (20 °C), **1**·2H_2O (−105 °C), **2**·2H_2O, **3**, and **4** (15 pages). Ordering information is given on any current masthead page.